The effect of recycling on the mechanical response of carbon fibres and their composites

Soraia Pimenta*, Silvestre T. Pinho

Department of Aeronautics, South Kensington Campus, Imperial College London. London SW7 2AZ, United Kingdom

Abstract

The development of processes for recycling carbon–fibre composite waste rises a question yet to be answered: how good can the performance of recycled composites be? This paper analyses fibres reclaimed in commercial facilities, and compares the performance of subsequently manufactured recycled woven composites to that of the virgin precursor (with the same fibre architecture). Different pyrolysis cycles resulted into different compromises between complete resin removal and full fibre strength retention. At the composite level, this paper shows how strength varies with the reclamation cycle, re-impregnation process and loading direction, while stiffness remains virtually unaffected. It is shown that composite tensile strength is favoured by gentle pyrolysis cycles generating little fibre damage, while compressive strength is fully retained after more aggressive cycles which completely remove the matrix. This work proves that the mechanical response of recycled composites can rival that of virgin precursors, while highlighting the benefits of application–driven optimisation of reclamation processes.

Keywords: Recycling, Carbon fibre reinforced polymers, Mechanical analysis.

1. Introduction

The last decade has seen a dramatic development of technologies for recycling Carbon–Fibre Reinforced–Polymers (CFRPs), but the full potential for re-using the recyclates in structural applications is yet to be realised. This paper investigates the effect of a commercial recycling process on CFRP, by comparing recycled and virgin materials at both the fibre and composite levels.

*Corresponding author.
Email address: soraia.pimenta@imperial.ac.uk (Soraia Pimenta)

Pimenta S, Pinho ST (2012). The effect of recycling on the mechanical response of carbon fibres and their composites. *Composite Structures* 94, 3669–3684. DOI:10.1016/j.compstruct.2012.05.024

Several methods to remove the resin and recover virgin–like fibres from composite waste have been developed [1, 2]. Amongst all, pyrolysis (thermal degradation in a controlled atmosphere) is currently the only process with a commercial implementation, run by ELG Carbon Fibre Ltd. (formerly Recycled Carbon Fibre Ltd., ELG-RCF) [3].

Pyrolysis conditions (temperature, atmosphere and processing time) have a strong influence on the quality of reclaimed carbon fibres [4]. Poorly–tuned processes result on fibre strength degradation (fibre stiffness is usually unaffected) or presence of residual matrix. Nonetheless, fibres recycled at small–scale processes usually recover more than 80% of the original stiffness and more than 90% of the original strength [4–6], suggesting that recycled carbon fibres can be re-used in structural applications [1].

This has driven efforts to re-impregnate recycled fibres with pristine resin, generally producing composites with discontinuous and complex architectures [7–10]. While these are very suitable to the typical unsized and unstructured form of reclaimed fibres, they inhibit a meaningful comparison between recycled and virgin composites, as the latter normally have a different fibre architecture.

Some recycling processes, e.g. ELG-RCF's conveyor–belt pyrolysis [3], can nevertheless preserve the virgin reinforcement architecture. This has been applied by Meredith et al. [11, 12] to recover structured fabrics from out–of–date woven prepreg rolls (which represent approximately 10% of the CFRP waste currently generated). The recycled weave was then prepreged and used to manufacture components of a racing car.

Despite all research on small–scale recycling processes [4–6] and discontinuous recycled composites [7–10], little is known about the performance of fibres reclaimed in commercial operations and the effect of recycling on woven composites. Recent work indicates that scaled up processes may induce additional fibre damage [13], although its impact at composite level has not been investigated. Only one recycled woven composite is so far characterised in the literature [12]; results suggest that fibre properties are not directly translated into composite performance.

This paper aims therefore at two complementary goals:

1. To assess the performance of carbon fibres reclaimed at an industrial plant by different pyrolysis cycles;
2. To understand the effect of fibre reclamation on composite performance, by comparing virgin and recycled composites with identical architectures.

The materials analysed in this study are identified in Section 2, and the experimental procedures described in Section 3. Results are presented in Section 4 and discussed in Section 5, so the main conclusions are summarised in Section 6.

2. Materials, recycling and manufacturing

2.1. Virgin material

The virgin (v) material (precursor to all recyclates) under investigation is a carbon–epoxy 2–D woven composite, supplied as prepreg for out–of–the–autoclave curing [14]. Material specifications are shown in Tables 1 (composite level) and 2 (fibre level).

Eight–ply laminates were laid–up and cured according to the manufacturer's instructions [14] for posterior analysis of the virgin composite. For single–filament analysis, a tow of virgin unsized fibres was used.

2.2. Fibre reclamation

Four small rolls of out–of–date virgin material were reclaimed by Recycled Carbon Fibre Ltd. (now ELG Carbon Fibre Ltd. [3]), using different pyrolysis cycles. This removed the (uncured) epoxy resin and recovered four different recycled fabrics (Table 3); owing to ELG-RCF's conveyer–belt process, the original weave architecture was preserved. All recycled (r) fibres (A, B, C and D) were analysed at the filament level.

2.3. Composite re-manufacturing

Two recycled fibre mats (r-B and D) were selected for re-manufacturing through resin film infusion (Table 3 and Figure 1), aiming to mimic the eight–ply virgin laminates. The same type of epoxy resin (HexPly M56 [14]) was used.

Each recycled *composite ply* was composed by one layer of recycled fibre mat and one layer of pristine resin film, matching the original resin content of the virgin prepreg (see area densities in Table 4). All recycled composite plies were individually vacuum–debulked to assist fibre–resin consolidation.

Laminate lay–up was performed as for the virgin material, ensuring a through–the–thickness homogenous distribution of the resin and laminate symmetry. Three recycled woven composites were manufactured, as specified in Table 3: materials r-B and r-D1 were cured as indicated by the resin manufacturer [14] (no external pressure applied), while r-D2 was cured under autoclave pressure to improve ply consolidation.

Table 1: Nominal specifications of the virgin composite prepreg [14].

Manufacturer	Reference	Fibre type	Resin type	Weave geometry	Fibre volume fraction, $\hat{V}^{\mathrm{f}}$
Hexcel	M56/37%/280H5/AS4–3K	AS4	M56	5 harness satin	52.7%

Table 2: Nominal specifications of the virgin carbon fibres [15].

Fibre description		Nominal fibre properties		
Manufacturer	Fibre type	Diameter (μm)	Stiffness (GPa)	Strength (GPa)
Hexcel	AS4	7.1	231	4.433

Table 3: Identification of materials used.

Fibre reference	Reclamation process$^{(\star)}$	Composite reference	Manufacturing process	Curing pressure
v	virgin	v	Prepreg curing	0 bar
r-A	ELG-RCF, cycle A	—	—	—
r-B	ELG-RCF, cycle B	r-B	Resin film infusion	0 bar
r-C	ELG-RCF, cycle C	—	—	—
r-D	ELG-RCF, cycle D	r-D1	Resin film infusion	0 bar
		r-D2	Resin film infusion	7 bar

$^{(\star)}$ Pyrolysis temperature is reduced from cycles A to D (all other process details are proprietary).

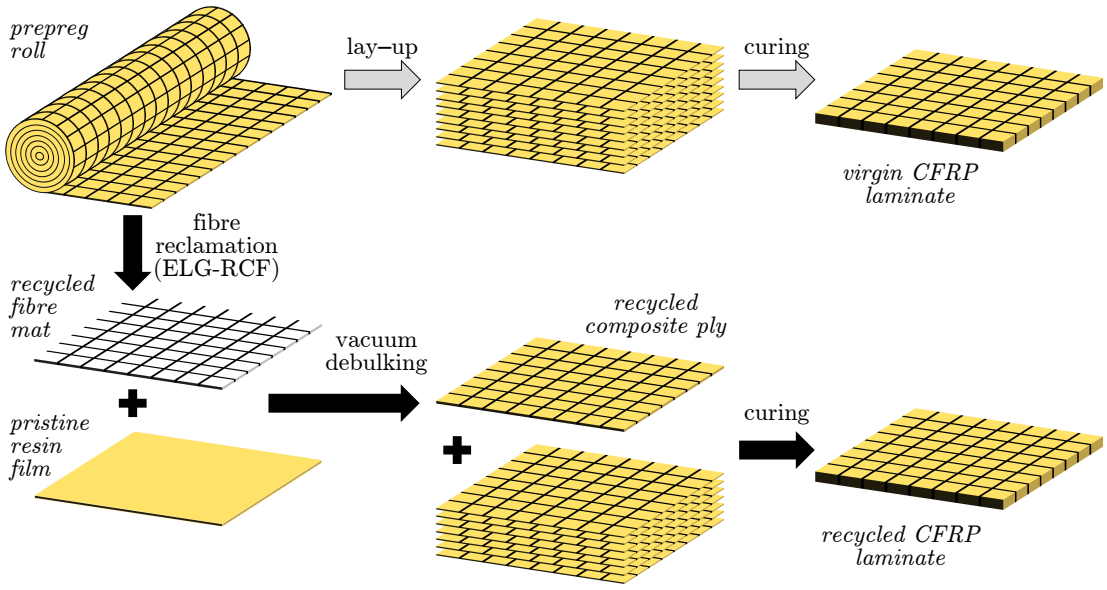

Figure 1: Fibre reclamation and composite (re-) manufacturing.

Table 4: Nominal densities of the virgin composite prepreg and its constituents [14].

Nominal property	Prepreg ply	Fibre (in prepreg)	Resin (in film)
Volume density, $\hat{\rho}_{\mathrm{V}}$ (g/cm^3)	1.50	1.79	1.17
Area density, $\hat{\rho}_{\mathrm{A}}$ (g/m^2)	444	280	164

3. Experimental analysis

3.1. Single–fibre analysis

3.1.1. Fibre inspection

The morphologies of all fibre types (virgin and recycled) were investigated through Scanning Electron Microscopy (SEM) of tows (taken from the centre of the reclaimed mats). Fibre diameters (ϕ^{f}) were measured (at $4,000\times$ magnification) in 25 filaments.

The area density ($\rho_{\mathrm{A}}^{\mathrm{f}}$) of each recycled weave was measured using a 120 mm$\times$100 mm sample (taken from the centre of the reclaimed mat). Similar samples were manually sheared until the tows locked-up (a dry orthogonal weave offers virtually no resistance to shear until parallel rotated tows become in contact), to assess the drapability and proneness to distortion of the recycled fabrics.

3.1.2. Single fibre tensile tests

The tensile strength of all fibre types (X^{f}, stochastic variable) were determined through Single–Fibre Tensile Tests (SFTTs). These were performed according to the BS ISO 11566 Standard [16], using in–house made grips and following the specifications shown in Table 5. Individual realisations of fibre strength (σ^{f}) were calculated using the average diameter of the corresponding fibre type.

As the strength of brittle fibres exhibits non–negligible scatter and length dependency [17], its characterisation requires estimating the strength distribution parameters for a chosen reference length. For each fibre type, the experimentally measured values of strength at two gauge lengths were fitted into a single Weibull distribution, defined as:

$$F_X(\sigma^{\mathrm{f}}) = 1 - \exp\left[-\frac{l}{\hat{l}} \cdot \left(\frac{\sigma^{\mathrm{f}}}{\hat{\sigma}_0^{\mathrm{f}}} \right)^m \right] \tag{1}$$

where m is the shape parameter (length independent), and $\hat{\sigma}_0^{\mathrm{f}}$ is the scale parameter for the reference length $\hat{l}$. For all fibre types, it was considered $\hat{l} = 15$ mm (mean nominal gauge length), and m and $\hat{\sigma}_0^{\mathrm{f}}$ were estimated through the maximum likelihood method (details are given in Appendix A).

Table 5: Specifications for single–fibre tensile tests.

Load cell	Type of glue	Fibre gauge length (mm)	Displacement rate (mm/min)	Number of tests (per fibre type)
10 N	3M Scotch–Weld 9323 B/A epoxy	10	0.1	≥ 25
		20	0.2	≥ 25

3.2. Composite analysis

3.2.1. Microscopy and composition

The through–the–thickness section of each laminate (v, r-B, r-D1 and r-D2) was analysed under an optical microscope.

The average thickness of each laminate ($\bar{t}$) was measured from the corresponding standard characterisation specimens (see Section 3.2.2). Volume fractions of fibres (V^{f}), matrix (V^{m}) and voids (V^{v}) were estimated using the measured composite thickness, measured fibre area densities ($\rho_{\mathrm{A}}^{\mathrm{f}}$), and nominal composite densities (shown in Table 4), according to the following expressions:

$$V^{\mathrm{f}} = \frac{\min\{\rho_{\mathrm{A}}^{\mathrm{f}}, \hat{\rho}_{\mathrm{A}}^{\mathrm{f}}\}}{\hat{\rho}_{\mathrm{V}}^{\mathrm{f}} \cdot \bar{t}}\,,\; V^{\mathrm{m}} = \min\left\{\frac{\max\{\rho_{\mathrm{A}}^{\mathrm{f}} - \hat{\rho}_{\mathrm{A}}^{\mathrm{f}}, 0\} + \hat{\rho}_{\mathrm{A}}^{\mathrm{m}}}{\hat{\rho}_{\mathrm{V}}^{\mathrm{m}} \cdot \bar{t}}, 1 - V^{\mathrm{f}}\right\}\,,\; V^{\mathrm{v}} = 1 - (V^{\mathrm{f}} + V^{\mathrm{m}}) \tag{2}$$

These are derived considering that (i) during recycling, significant amounts of residual resin are associated with negligible fibre loss (and vice–versa), and (ii) during cure, significant matrix bleeding may occur only after full impregnation.

3.2.2. Mechanical testing

The in–plane mechanical properties of the four composites were measured according to the specifications in Table 6 (whereby T, C and S respectively represent tension, compression and shear). For tension and compression, the same number of specimens were tested in the warp and weft directions (respectively represented by 1 and 2). All specimens were end–tabbed and equipped with strain gauges; both faces of compression specimens were instrumented to monitor bending.

The data reduction method for the $\pm 45^{\circ}$ shear tests was adapted from the original standard [20] to account for large deformations (see full derivation in Appendix B). From the testing data (longitudinal deformation ε_{L}, transverse deformation ε_{T} and load P), true shear deformations (γ_{12}) and shear stresses (τ_{12}) along fibre direction were calculated as:

Table 6: Specifications for the standard mechanical characterisation (gauge section dimensions).

Test case	Stacking sequence	Length (mm)	Width (mm)	Disp. rate (mm/min)	Valid tests (per direction) v	r-A	r-D1	r-D2
T[18]	$[0_4]_{\mathrm{s}}$ or $[90_4]_{\mathrm{s}}$	192	25	2.0	20	6	5	6
C[19]	$[0_4]_{\mathrm{s}}$ or $[90_4]_{\mathrm{s}}$	7	19	1.0	24	6	6	6
S[20]	$[\pm 45_2]_{\mathrm{s}}$	192	25	2.0	21	6	6	6

$$\gamma_{12} = 2 \cdot \operatorname{atan}\left(\frac{\varepsilon_{\mathrm{L}} + 1}{\varepsilon_{\mathrm{T}} + 1}\right) - \frac{\pi}{2} \qquad \text{and} \qquad \tau_{12} = \frac{1}{2} \cdot \frac{P}{t_0 \cdot w_0 \cdot (1 + \varepsilon_{\mathrm{T}})} \cdot \cos(\gamma_{12}) \tag{3}$$

where t_0 and w_0 are the initial specimen's thickness and width. When the operational strain gauge range was exceeded ($|\varepsilon| \gtrsim 4\%$), γ_{12} was extrapolated linearly in time.

3.2.3. Fractography

Tensile and shear failure mechanisms were investigated in post–mortem fracture surfaces. Compressive failure was analysed in reduced compact compression specimens, by optical microscopy of several post–mortem cross sections (Figure 2) [10, 21].

4. Results

4.1. Single–fibre analysis

4.1.1. Fibre morphology

The throughput of different recycling processes is analysed in Figure 3. When compared to the virgin fabric, the most aggressive process (A) yielded a lighter weave with significantly thinner fibres. On the contrary, fibres reclaimed by process D (the least aggressive one) showed no statistically significant variation of diameter, and a small increase of area density (which indicates the present of residual resin). Processes B and C produced intermediate results.

Figure 4 shows that, as the reclamation process becomes more aggressive (from D to A), the weaves become more drapable but also more susceptible to distortion.

The morphology of virgin and reclaimed fibres is analysed in Figure 5. Process A (Figure 5b) induced extensive and severe pitting on the fibres, as well as an irregular surface. Fibres r-B (Figure 5c) show surface damage and a burnt aspect, but only

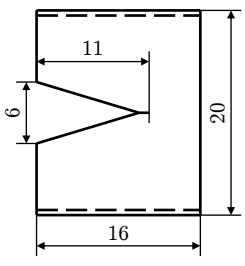

(a) Specimen geometry (dimensions in mm).

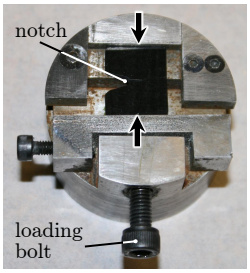

(b) Test setup.

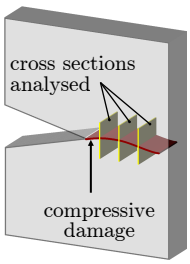

(c) Cross sections analysed under the optical microscope.

Figure 2: Reduced compact compression specimens for study of compressive damage.

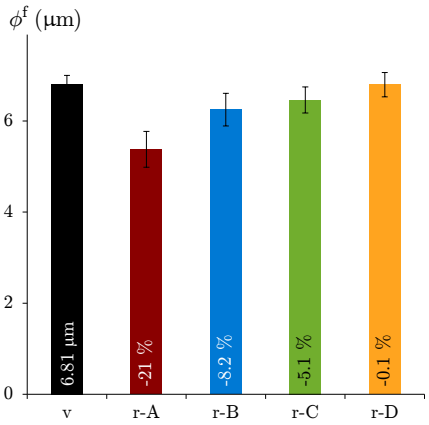

(a) Fibre diameters (percentage reduction indicated; error bars represent one standard deviation).

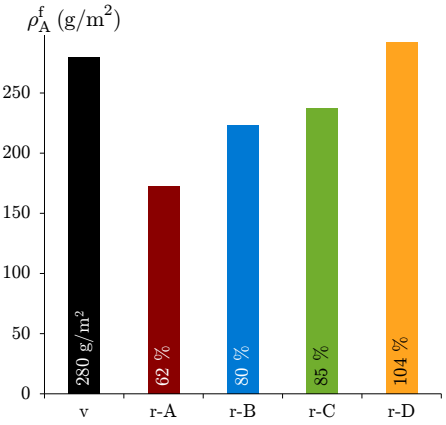

(b) Area density of fibre mats (percentage retention after reclamation indicated).

Figure 3: Fibre yield after pyrolysis (virgin–fibre properties indicated for reference).

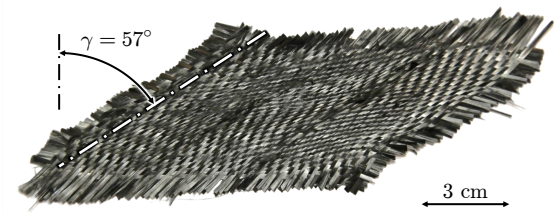

(a) r-A.

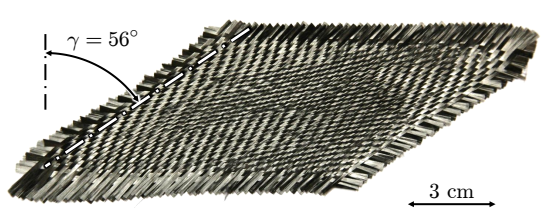

(b) r-B.

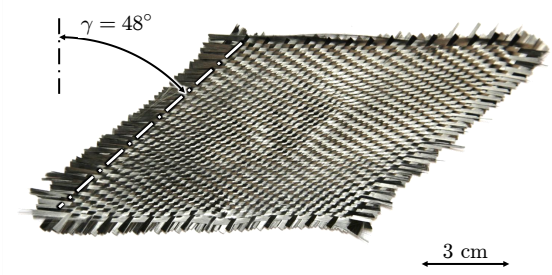

(c) r-C.

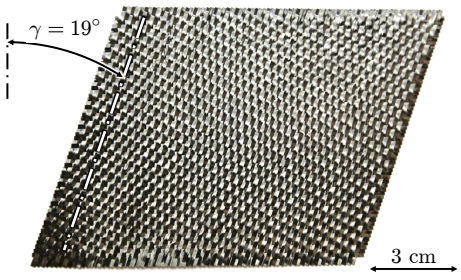

(d) r-D.

Figure 4: Recycled fabrics sheared manually up to the lock-up point.

occasional and mild pitting. Process C (Figure 5d) left minimal quantities of residual resin on an otherwise smooth fibre surface, with occasional mild pitting. The least aggressive cycle (D, Figure 5e) produced tows with alternate regions of (i) virgin–like fibres and (ii) fibres covered by a thin layer of residual resin with imprints of transverse filaments.

4.1.2. Mechanical properties

Figure 6a shows the average and standard deviations of fibre strengths measured by SFTTs. A clear size effect is present in all fibre types, which validates the use of a simple model neglecting end–effects for the comparative purpose of this analysis [17]. Reclaimed fibre types A, B and C evidenced a substantial strength degradation relatively to the virgin precursor, slightly more severe at the larger gauge length. In contrast, process D recovered fibres with nearly full strength retention.

Weibull plots with experimental and fitted single fibre strengths for all fibre types are presented in Figures 6b–6f (same scale used for comparison). To include measurements at both gauge lengths, each strength realisation σ_i at length l_i is shown normalised to $\hat{l} = 15$ mm as:

$$\hat{\sigma}_i = \left(\frac{l}{\hat{l}}\right)^{1/m} \cdot \sigma_i \tag{4}$$

Weibull parameters (including m used in Equation 4) of fitted distributions are shown in Table 7, as well as the corresponding expected value ($\mu_{\hat{X}}$) and Coefficient of Variation (CoV). The quality of fitting between the maximum likelihood Weibull distribution and experimental data is very good for all fibre types (Figures 6b–6f).

The variability of fibre strength increased substantially after reclamation (Table 7). While this effect was magnified for the most aggressive processes, it was still considerable when no significant strength degradation was observed (process D).

Table 7: Maximum likelihood Weibull fitting to SFTT stength (for $\hat{l} = 15$ mm).

Fibre type	m	$\hat{\sigma}_0$ (GPa)	$\mu_{\hat{X}}$ (GPa)	CoV (%)
v	9.34	4.954	4.699	12.8
r-A	1.99	0.839	0.744	52.5
r-B	2.91	1.130	1.007	37.4
r-C	2.87	1.462	1.303	37.8
r-D	4.77	4.988	4.567	23.9

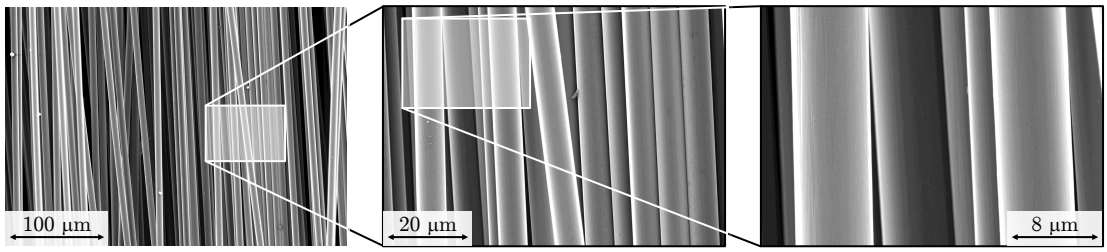

(a) Fibres v.

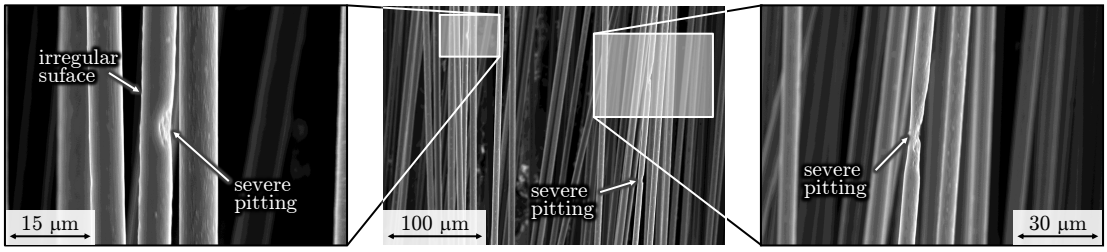

(b) Fibres r-A.

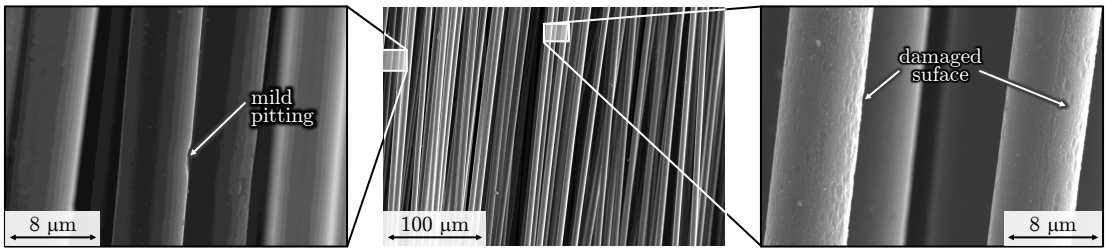

(c) Fibres r-B.

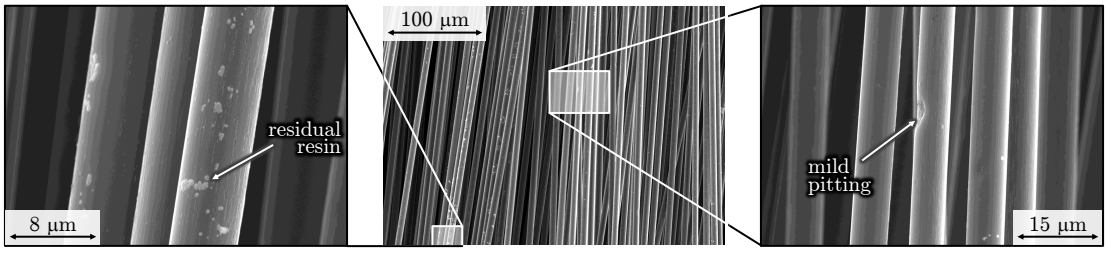

(d) Fibres r-C.

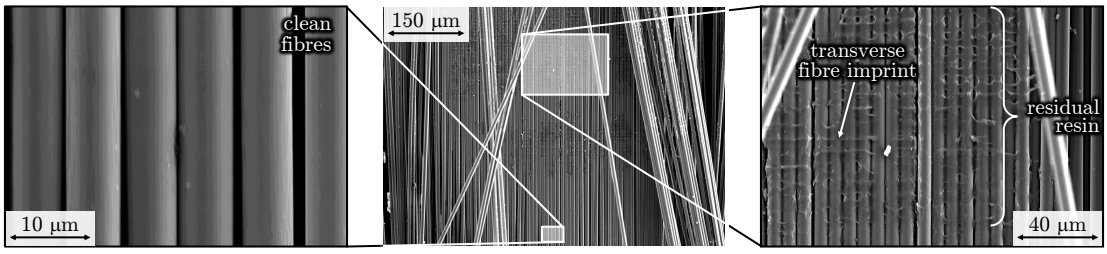

(e) Fibres r-D.

Figure 5: Scanning–electron micrographs of virgin and recycled carbon fibres.

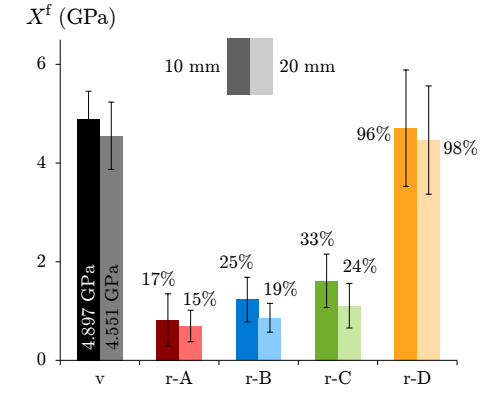

(a) Fibre strength statistics (average strength retention indicated; error bars represent one standard deviation).

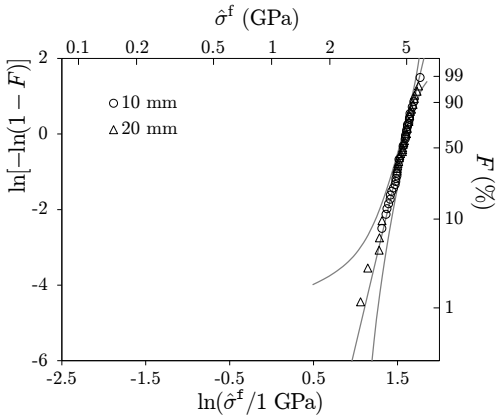

(b) Weibull plot for fibres v.

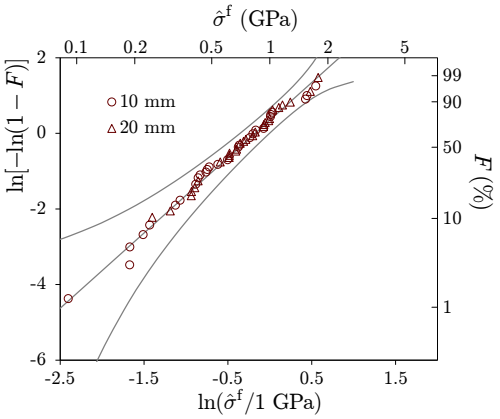

(c) Weibull plot for fibres r-A.

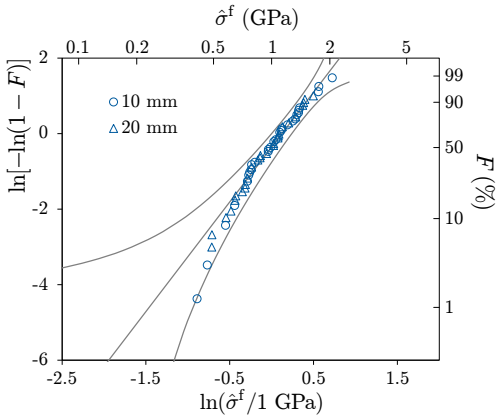

(d) Weibull plot for fibres r-B.

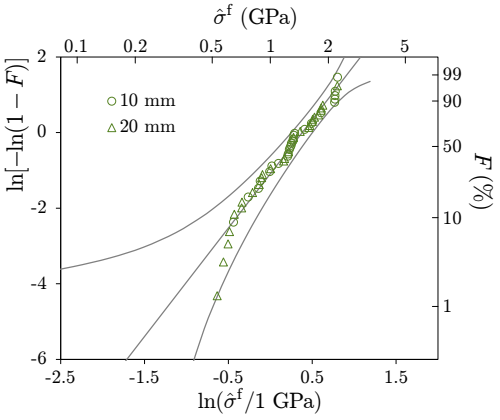

(e) Weibull plot for fibres r-C.

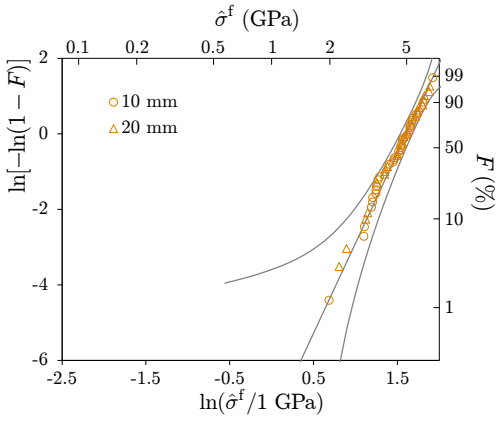

(f) Weibull plot for fibres r-D.

Figure 6: Tensile strengths of the virgin and recycled fibres. The Weibull plots feature strength distributions normalised for $\hat{l} = 15$ mm (95% confidence intervals for percentiles are presented as well).

4.2. Composite analysis

4.2.1. Morphology

For each composite manufactured, Figure 7 shows the average thickness and composition (in terms of fibre, resin and void content), while Figure 8 analyses the morphology of a representative cross section.

Recyclate B presented a slightly lower fibre content than that of the virgin material, although it was considerably thinner (Figure 7) due to fibre loss during reclamation (Figure 3). Virtually no voids were found, even where fibres were very tightly packed (Figure 8b).

Following the standard out–of–the–autoclave re-manufacturing cycle with weave D (material r-D1) resulted in a very high void content and poor compactation both at ply and tow levels (Figures 7 and 8c). Applying typical autoclave pressure levels (7 bar, as indicated for Hexcel HexPly AS4–8552 [22]) in material r-D2 greatly reduced void content, although the laminate was still thicker and had a lower fibre fraction than the virgin precursor (Figures 7 and 8d).

4.2.2. Mechanical properties

The elastic properties (unidirectional moduli E, in-plane shear modulus G_{12}, Poisson's ratio ν_{12}) and strengths (X for unidirectional, S_{12} for in-plane shear) of the virgin and recycled composites are presented in Tables 8 and 9. Figure 9 shows the average (represented by an overbar) retention of stiffness and strength for each recycled composite relatively to the virgin precursor; confidence intervals for the ratios are based on Fieller's theorem [23] (see Appendix C for details).

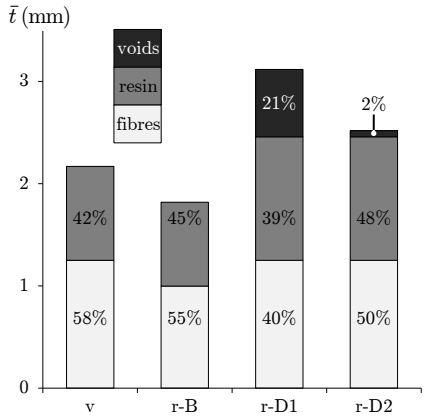

Figure 7: Thickness and constituent volume fraction of virgin and recycled composites.

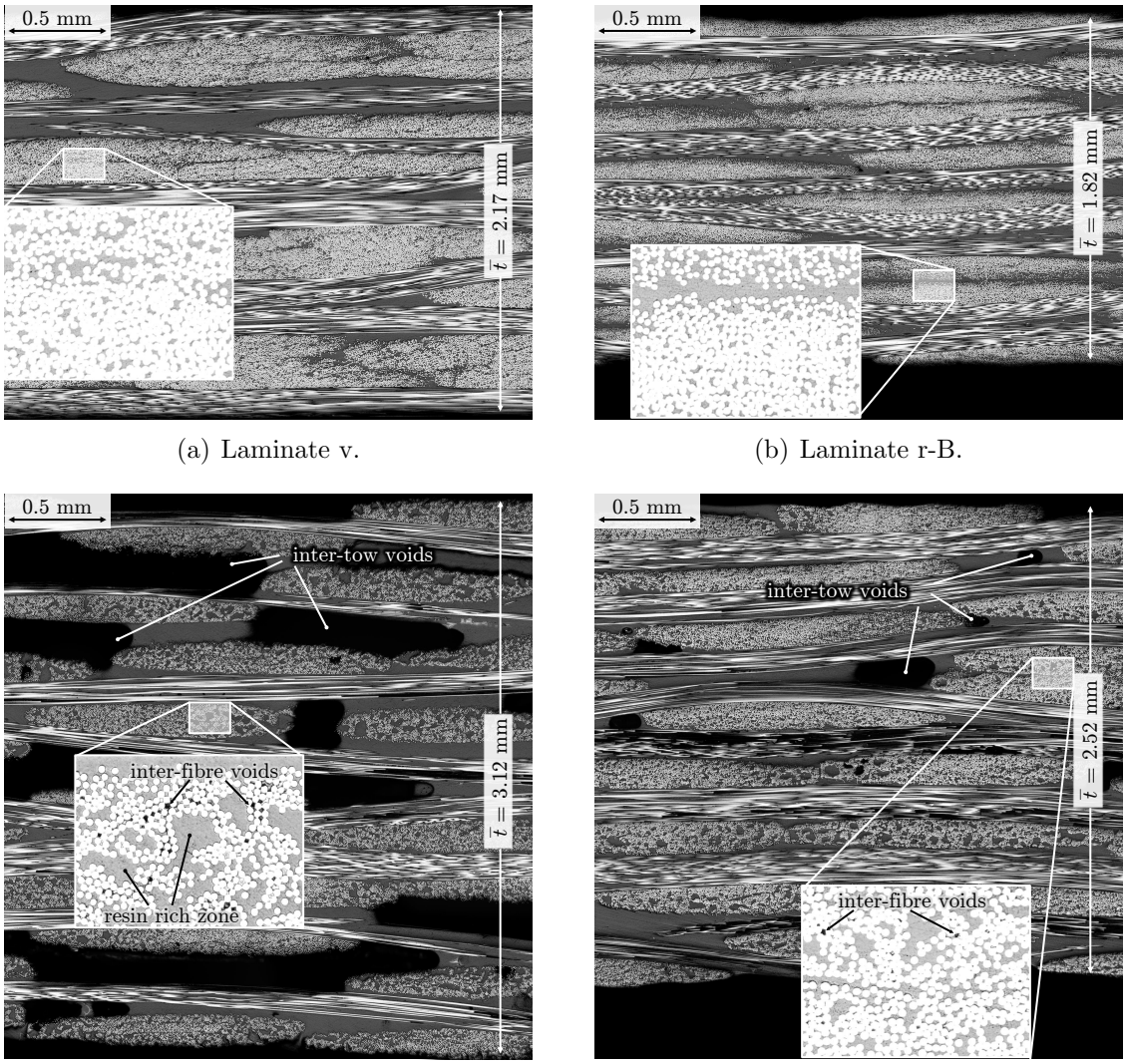

(a) Laminate v.

(b) Laminate r-B.

(c) Laminate r-D1.

(d) Laminate r-D2.

Figure 8: Micrographs of through–the–thickness cross sections of virgin and recycled composites. (Brightness and contrast of zoom–ins were adjusted to enhance voids.)

Table 8: Elastic properties of virgin and recycled composites (considering true specimen thicknesses).

Material	E_{T1} (GPa)	E_{T2} (GPa)	E_{C1} (GPa)	E_{C2} (GPa)	G_{12} (GPa)	ν_{12} (–)
v	69.3 ± 1.7	67.5 ± 1.2	62.4 ± 1.8	62.2 ± 2.3	4.6 ± 0.1	0.05 ± 0.01
r-B	65.9 ± 1.8	63.9 ± 1.5	59.6 ± 2.1	61.2 ± 3.0	5.2 ± 0.3	0.05 ± 0.01
r-D1	47.3 ± 1.2	43.1 ± 1.3	43.8 ± 3.1	46.5 ± 4.5	2.7 ± 0.1	0.07 ± 0.03
r-D2	55.9 ± 1.4	56.2 ± 0.6	53.7 ± 1.9	53.4 ± 2.0	3.7 ± 0.1	0.02 ± 0.01

Table 9: Strengths of virgin and recycled composites (considering true specimen thicknesses).

Material	X_{T1} (MPa)	X_{T2} (MPa)	X_{C1} (MPa)	X_{C2} (MPa)	S_{12} (MPa)
v	932 ± 46	1000 ± 53	681 ± 56	733 ± 56	133.5 ± 6.9
r-B	271 ± 17	257 ± 15	694 ± 45	729 ± 33	92.9 ± 3.2
r-D1	476 ± 12	390 ± 25	223 ± 19	255 ± 14	42.5 ± 1.6
r-D2	634 ± 30	640 ± 44	383 ± 38	373 ± 17	72.7 ± 2.9

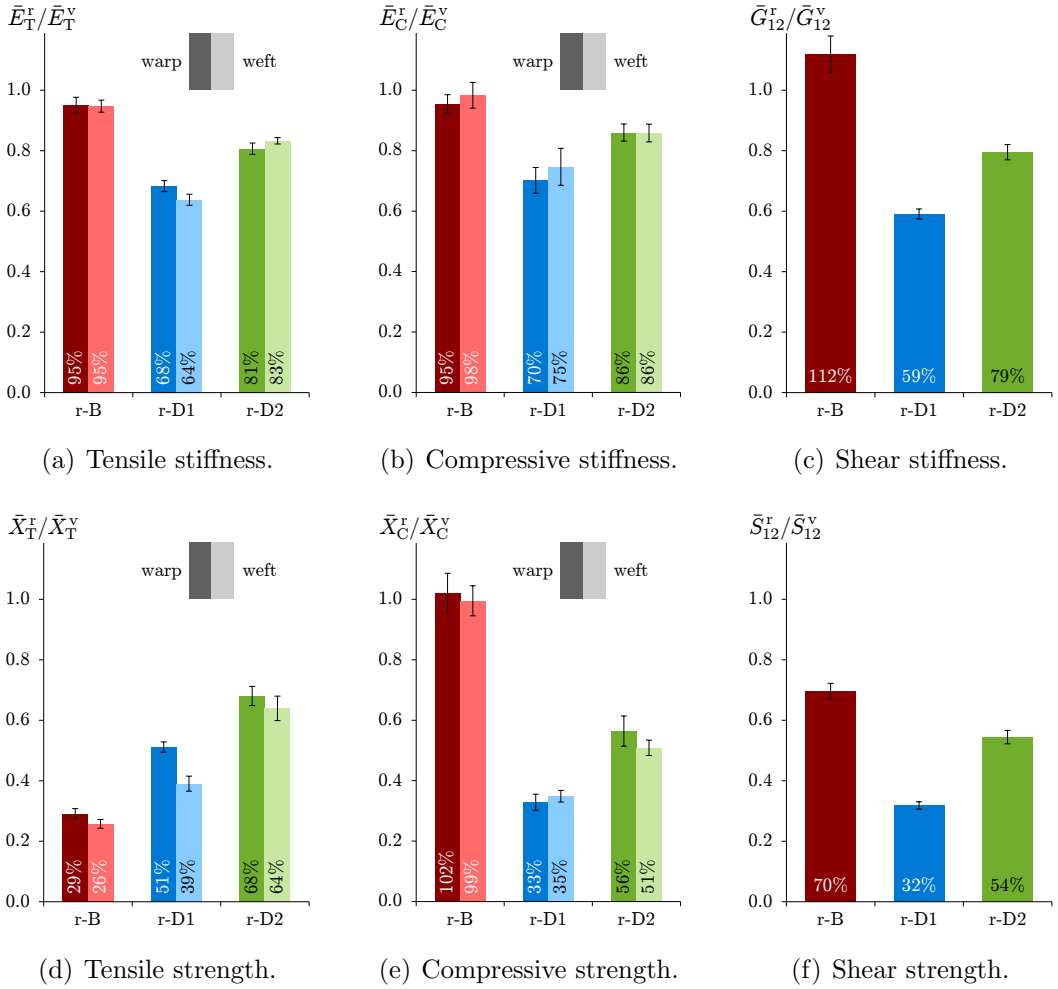

(a) Tensile stiffness. (b) Compressive stiffness. (c) Shear stiffness.

(d) Tensile strength. (e) Compressive strength. (f) Shear strength.

Figure 9: Ratio between mean properties of recycled and virgin composites, considering true specimen thicknesses. Error bars represent 95% confidence intervals.

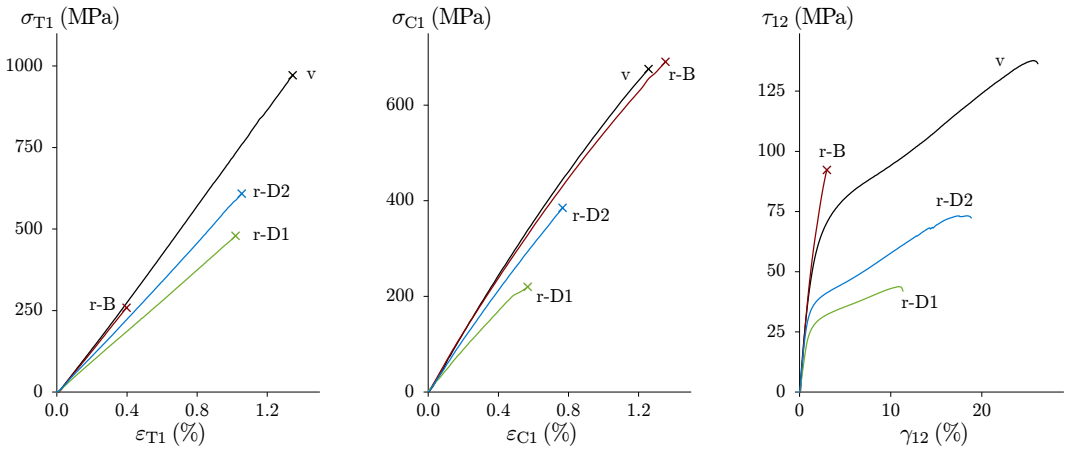

(a) Tension. (b) Compression. (c) Shear.

Figure 10: Typical stress–strain curves for virgin and recycled composites (symbol × corresponds to catastrophic failure).

The mechanical performance of recycled composites (Figure 9) depended on three factors: (i) fibre reclamation process, (ii) laminate re-manufacturing process, and (iii) loading case. The stiffness of composite r-B was very close to that of the virgin material in all loading cases; in contrast, materials r-D1 and r-D2 were significantly softer (especially the former). Regarding strength, the recyclates underperformed the virgin precursor in all cases but composite r-B under compression; material r-D2 (cured at 7 bar) was consistently stronger than material r-D1 (cured at 0 bar). Warp and weft performances were similar, although tensile strength retention was slightly higher in the former.

A typical stress–strain curve for each material and loading case is reproduced in Figure 10. The response of all composites under tension was linear up to catastrophic failure (Figure 10a). Under compression, a progressive decrease of stiffness with increasing strains was observed in all cases; failure was catastrophic as well (Figure 10b). Composites v, r-D1 and r-D2 were markedly non–linear under ±45° shear, with progressive failure; on the contrary, composite r-B sustained a nearly–linear behaviour up to higher stresses, but failed catastrophically (Figure 10c).

4.2.3. Damage morphology

Figure 11 shows representative fracture surfaces of the composites tested under different loads; no significant difference was found between warp and weft directions.

Under tension, the virgin composite (Figure 11a) failed by fracture of all load–

aligned tows within a narrow area, with considerable pull–out but very little delamination and defibrillation. The fracture surfaces of recyclate B were extremely smooth, with virtually no pull–out, delamination or defibrillation (Figure 11d). The opposite was observed in composite r-D1 (Figure 11g), where large delaminations (frequently along the entire gauge length) joined individual ply failures with extensive splitting of both longitudinal and transverse tows. Material r-D2 (Figure 11j) presented a fracture surface more similar to that of the virgin composite, although with significantly more defibrillation of tows and delamination.

Under compression, the virgin composite (Figure 11b) failed by fibre kinking in load–aligned tows, splitting of transverse tows, and delamination; these features formed a narrow damage band inclined through the thickness. Composite r-B presented a remarkably similar damage morphology to the virgin counterpart (Figure 11e). In contrast, composite r-D1 (Figure 11h) failed mainly by coalescence of voids into extensive delaminations; tow splitting and kinking occurred only occasionally and later in the process. Recyclate D2 (Figure 11k) presented damage features similar to those of the virgin material, but spread over a larger area under the influence of manufacturing voids.

Under shear, the virgin composite (Figure 11c) evidenced ductile failure by scissoring of defibrillated tows; virtually no fibre breakage occurred. Reyclate B presented brittle tow failure, following either the normal to the loading (90°) or the fibre (45°) direction (Figure 11f). Materials r-D1 (Figure 11i) and r-D2 (Figure 11l) presented similar features to the virgin composite, although with less extensive defibrillation.

5. Discussion

5.1. Defects in reclaimed fibres

Following the fibre analysis presented in Section 4.1, Table 10 summarises the typical defects that can be expected after pyrolysis, depending on the intensity of the cycle.

Selecting the adequate processing conditions is a trade–off between (i) complete matrix removal and (ii) retention of fibre properties. Previous research [4, 5] has shown that laboratory / pilot scale reclamation processes can fulfil both conditions simultaneously. However, this may not be feasible at commercial scales as well.

Fibre types r-A, r-B and r-C underwent too aggressive cycles, with significant fibre degradation and strength reduction (Figures 3–6). Fibre stiffness was not affected by reclamation, as evidenced by the full retention of modulus in composite r-B (Figure 9a).

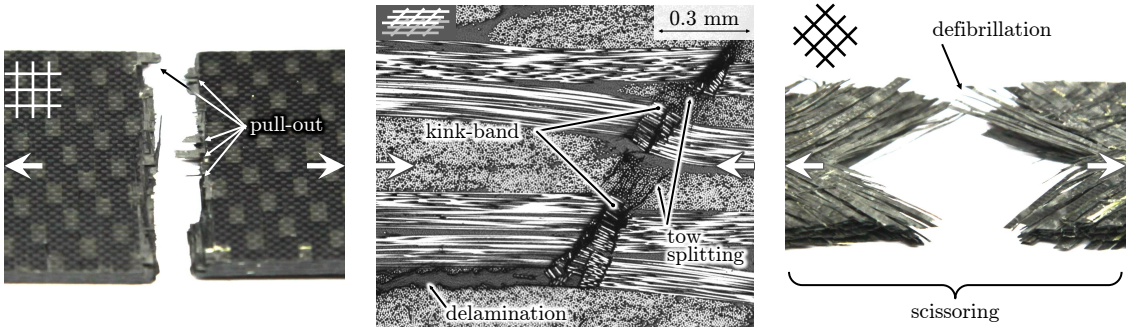

(a) v under tension. (b) v under compression. (c) v under shear.

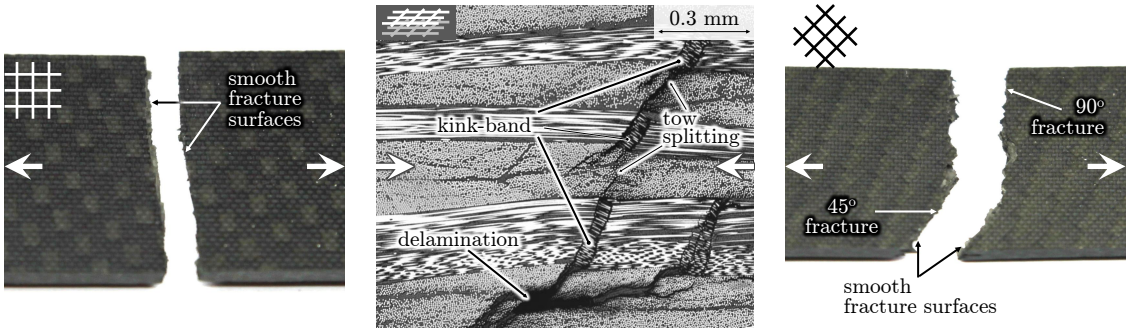

(d) r-A under tension. (e) r-A under compression. (f) r-A under shear.

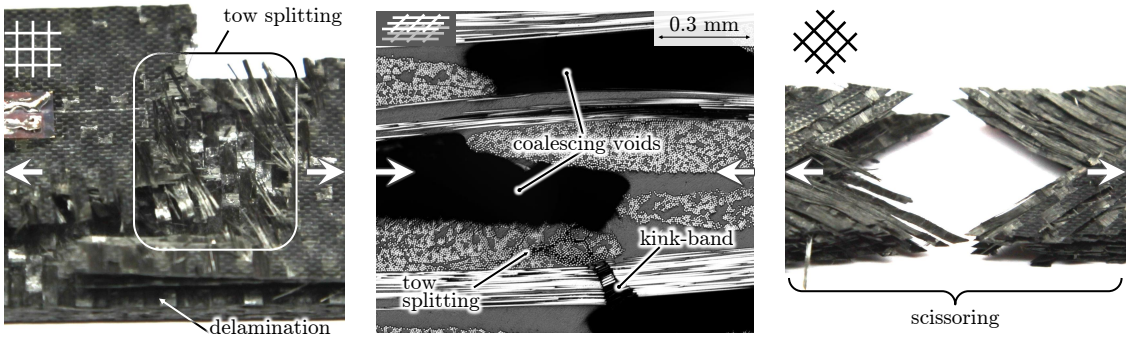

(g) r-D1 under tension. (h) r-D1 under compression. (i) r-D1 under shear.

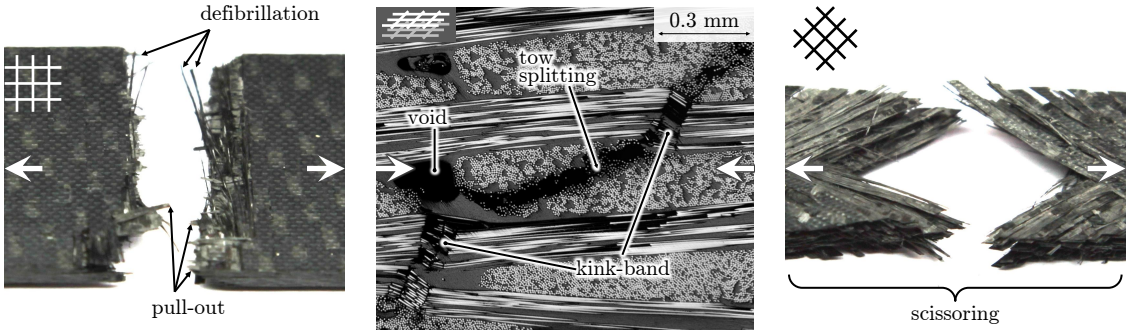

(j) r-D2 under tension. (k) r-D2 under compression. (l) r-D2 under shear.

Figure 11: Damage morphology in virgin and recycled composites. For each case, load direction and tow orientation are represented respectively by white arrows and a grid.

Table 10: Qualitative assessment of typical defects in fibres reclaimed by different pyrolysis cycles.

Fibre defect	Pyrolysis reclamation cycle		
	Too aggressive (e.g. A, B, C)	Ideal cycle	Too gentle (e.g. D)
Diameter reduction (Figure 3a)	●●	○	○
Fibre loss (Figure 3b)	●●	○	○
Pitting (Figure 5)	●●	○	○
Surface damage (Figure 5)	●●	○	○
Residual matrix (Figure 5)	○	○/●	●●
Stiffness reduction (Figure 12a)	○	○	○
Strength reduction (Figure 6a)	●●	○/●	○
Increase of strength CoV (Table 7)	●●	●	●

Key: ○ – none / negligible; ● – minor; ●● – major.

On the contrary, fibre type r-D showed no signs of degradation, but it is estimated that 7.6% of the original resin content was still present (Figures 3 and 6). This was sufficient to make the weave very stiff (Figure 4d); nevertheless, SEM observations show many clean fibres (Figure 5e), and individual fibres could be easily separated.

5.2. Through–the–thickness heterogeneity in reclaimed fibre mats

Figure 5e suggests that reclamation was heterogeneous in the through–the–thickness direction of the fabric. During pyrolysis of a woven prepreg, the surface of each tow is either directly exposed to the heat and gas flow, or shielded by the presence of a perpendicular tow. This resulted, for material r-D, into alternating regions of very clean fibres and residual matrix, separated by the tow crimp line.

The weave used in this work (5 harness satin) has a warp–dominated face and a weft–dominated one. The through–the–thickness heterogeneity evidenced in Figure 5e could thus result into different fibre properties along the warp and weft directions, for all recyclates. This is a possible justification for the slightly different tensile strength retentions at the composite level in the two material directions (Figure 9d).

5.3. Fibre strength retention after reclamation

Fibre strength was severely degraded by processes A, B and C, with pyrolysis temperatures ranging between 500 to 700°C. This is consistent with previous reports of fibre oxidation under the presence of oxygen for temperatures above 600°C [4].

The strength distributions of recycled fibres evidence a good fitting with Weibull's theory (Figure 6c–f) and the presence of size effects. This, combined with the larger

strength variability of recycled fibres, resulted in a reduction of strength retention with increasing gauge length (Figure 6a).

Figures 6b and 6f suggest that a part of the population of r-D fibres is stronger than the corresponding virgin population. This unexpected behaviour can be due to either (i) the presence of a layer of residual matrix on some recycled fibres (as seen in Figure 5e), or (ii) an artifact from testing (e.g. different stress concentrations at fibre ends, statistical variance). The possibility of having inadvertently tested two fibres together can be discarded, as it is not corroborated by the experimental data.

5.4. Influence of the fibre reclamation process on the composite performance

Figure 12 shows the relation between (i) the retention of average fibre strength (averaged between both gauge lengths) and (ii) the retention of average composite properties (averaged between warp and weft directions for tension and compression) after recycling. Given the different fibre contents of the four laminates tested (Figure 7), the real effect of reclamation is better captured considering all properties normalised to $\hat{V}^{\mathrm{f}} = 52.7\%$. Table 11 summarises the influence of fibre reclamation defects on the mechanical response of recycled composites, as discussed below.

Composite stiffness (Figures 12a–c) was only slightly affected by the reclamation process (although obviously affected by fibre content after re-manufacturing). This confirms that fibre stiffness was fully recovered, even when strength was severely degraded. Nevertheless, the weave is more prone to distortion after more aggressive cycles (Figure 4), hence the small reduction of tensile and compressive stiffnesses and apparent increase of $\pm 45^{\circ}$ shear stiffness associated with severe fibre degradation (Table 11).

Regarding strength, the effect of weave distortion is not likely to overcome the effect of naturally existing crimp regions, which appears to be characterised by similar crimp angles in both virgin and recycled laminates (Figure 8). However, the effect of fibre strength on composite strength is very pronounced and complex (Figures 12d–f).

Table 11: Influence of recycled–fibre defects on composite performance (for normalised fibre content).

Reclamation defect	Composite defect	Influence on properties E, G	X_{T}	X_{C}	S_{12}
Fibre degradation (r-B)	Fibre strength reduction	○	●●	○	●● / ○
	Mild weave distortion	●	○	○	○
Residual matrix (r-D)	Weak interface / interlayer	○	○	●●	●● / ○
	Difficult compactation / voids	○	●●	●●	●●

Key: ○ – none / negligible; ● – minor; ●● – major.

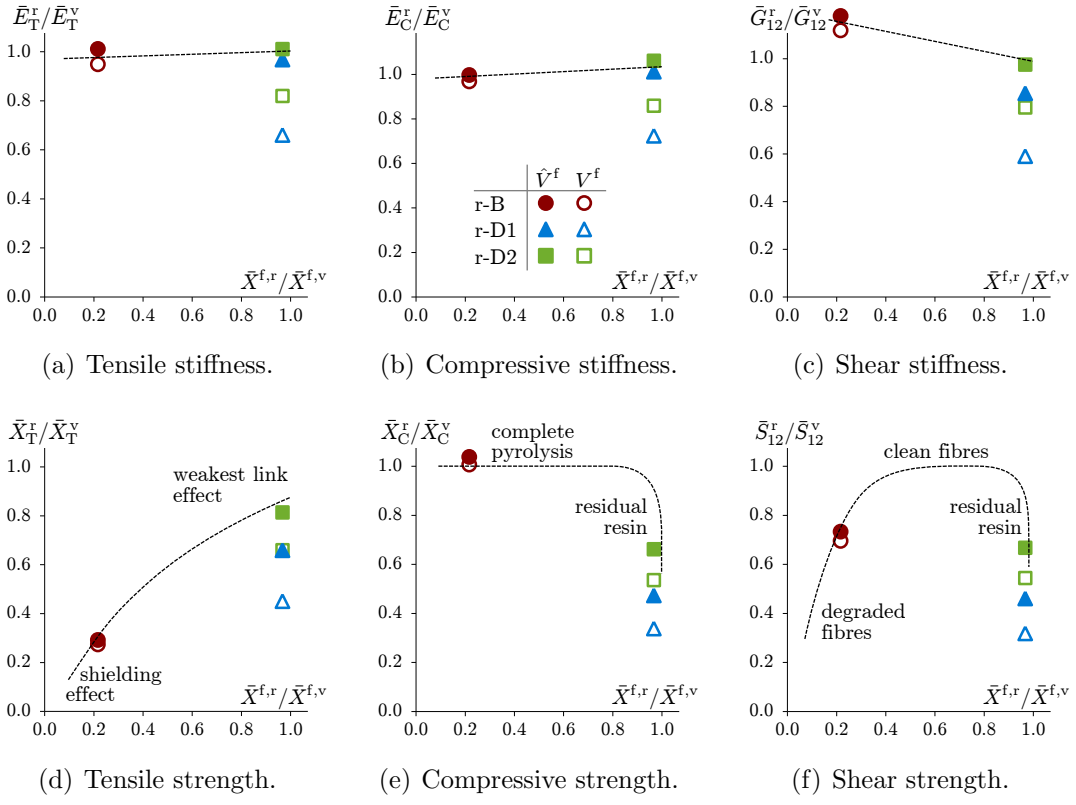

(a) Tensile stiffness. (b) Compressive stiffness. (c) Shear stiffness.

(d) Tensile strength. (e) Compressive strength. (f) Shear strength.

Figure 12: Retention of mechanical properties at the composite level versus retention of fibre strength: experimental measurements (data points, considering either the true fibre content, V^{f}, or the nominal one, $\hat{V}^{\mathrm{f}}$) and suggested trends (dashed lines).

5.4.1. Tensile failure

Tensile failure in woven composites is dominated by fibre fracture in load–aligned tows [24]. This is illustrated in Figure 12d, where tensile strength at the composite level correlates well with fibre strength. Comparing the normalised ($\hat{V}^{\mathrm{f}}$) strength retentions of materials r-D1 and r-D2 suggests the higher void content and poorer impregnation in the former also contribute to strength degradation, by triggering delaminations and smearing failure (Figures 11g and 11j).

The presence of the matrix and the stochastic nature of fibre strength are important as well [25]. For very degraded fibres (e.g. r-B), the weakest ones in the composite will fail at very low stresses; however, the resin will withhold the damage in a confined region, thus *shielding* the stronger fibres from stress concentrations (Figure 12d).

For barely degraded fibres (e.g. r-D), variability of strength is nevertheless higher than in the virgin precursors (Table 7). The *weakest* fibres will thus fail prematurely, but at stress levels sufficiently high to promote matrix splitting, large stress concentrations

and, consequently, structural failure (Figure 12d).

5.4.2. Compressive failure

Although compressive failure mechanisms in woven composites constitute still an active field of research, some authors defend that kink–band initiation — and, consequently, compressive strength — is dictated by the architecture and strengths of the resin and interface, but not by the strength of the fibres themselves [26–29]. This is strongly supported by the results here obtained.

On the one hand, virgin and r-B composites show virtually identical compressive strengths (Figure 9e) and damage morphologies (Figures 11b,e). This proves that compressive failure was insensitive to a 78% fibre strength degradation; it also suggests the fibre–matrix interface in the recyclate to be as strong as that in the virgin material.

On the other hand, composites r-D1 and r-D2 evidenced residual resin (Figure 3b) and a poor impregnation (Figures 8c–d), both susceptible to result in a weak fibre–matrix interface (or in a weak *interlayer* of partially pyrolysed matrix between fibres and pristine resin). This caused a significant reduction of compressive strength, further affected by the presence of voids and delaminations (Figures 12e and 11h,k).

It is envisaged in Table 11 and Figure 12e that very aggressive reclamation cycles will severely degrade fibre strength but *completely pyrolyse* the matrix, hence potentially resulting in a total recovery of compressive strength at the composite level. Too gentle cycles will preserve fibre strength, but leave *residual resin*; therefore, the fibre–matrix interface (or interlayer) will have degraded properties and, consequently, the composite compressive strength should decrease.

5.4.3. Shear failure

Under $\pm 45^{\circ}$ shear, two independent failure modes were observed (Figure 11); both are considered in Table 11 and Figure 12f as detailed below:

- Severely *degraded fibres* will lead to premature tensile failure of the tows, as seen in material r-B (Figure 11f). This composite withstood nevertheless the linear behaviour up to slightly higher stresses than the virgin one (Figure 10c); this could suggest an improved fibre–matrix interface, although it may also be simply related to the higher shear modulus measured (Figure 12c).
- Composites with stronger fibres will enter the non–linear region, after which resin and fibre–matrix interface dominate the response. *Clean fibres* should yield composites with good fibre–matrix adhesion and, consequently, large shear strength.

A too gentle pyrolysis cycle (e.g. D) will originate *residual resin*, thus reducing the adhesion and the composite shear strength (Figure 12f).

5.5. Analysis of the re-manufacturing process

The dissimilar morphologies observed in the different recycled composites (Figure 8) show that the specific fibre reclamation cycle affects composite re-manufacturing and the quality of re-impregnation. This effect, mainly related to the presence of residual matrix in reclaimed fibres, is summarised in Table 12 and discussed below.

On the one hand, in the absence of residual matrix, recycled weave r-B was successfully re-impregnated by out–of–the–autoclave resin infusion. The composite presented virtually no voids and a high fibre content (Figures 7 and 8b), suggesting similar resin flow, ply nesting and compactation as in the virgin precursor.

It was previously concluded (Sections 5.4.2 and 5.4.3) that cycle B did not degrade the fibre–matrix interfacial strength. This agrees with previous results obtained for single–fibre and short–fibre composites [7, 10] and proves that, from a structural point of view, re-sizing is not necessary after full pyrolysis of the resin.

On the other hand, a too gentle pyrolysis cycle yields residual matrix; this limits resin flow, compactation and fibre wetting during re-impregnation. With no external pressure applied, composite r-D1 presented a low fibre volume fraction and high void content (Figure 7), with consequent loss of performance (Figures 12).

Applying the typical autoclave curing cycle (7 bar external pressure) eased most problems in recyclate r-D2. However, fibre content was still lower than in the virgin material due to insufficient compactation (Figure 7), and voids were still present (albeit at a much smaller scale, Figure 8d). Further improvements should be obtainable by increasing the pressure during cure, and/or re-prepreging the weave beforehand.

As mentioned in Sections 5.4.2 and 5.4.3, the marked decrease in compressive and shear strengths in materials r-D1 and r-D2 indicates an apparently weaker fibre–matrix

Table 12: Relation between fibre reclamation cycle and manufacturing defects.

	Composite material →	r-B	r-D1	r-D2	Ideal
Process	Intensity of reclamation cycle	Too aggressive	Too gentle		Ideal
	Additional manufacturing pressure	○	○	●	○/●/●●
Defects	Presence of residual matrix	○	●	●	○/●
	Void content	○	●●	●	○
	Degradation of interface / interlayer	○	●●	●	○/●

Key: ○ – none / negligible; ● – minor; ●● – major.

interface (or interlayer) when residual resin is present. This may nevertheless be the result of incomplete fibre wetting, as evidenced in Figures 8c and 8d.

5.6. Quality control and optimisation of recycling processes

One of the key aspects for the success of CFRP recycling for high–performance applications is guaranteeing the quality of the recycled fibres; this is usually assessed by their strength retention.

However, measuring fibre strength directly has the disadvantages associated with SFTTs; for recycled fibres, statistical significance can be further compromised because the effects of reclamation are not uniform in the through–the–thickness direction (see Section 5.2). Nevertheless, the good agreement observed between the tensile strength retention of single fibres and that of composites (Figure 12d) shows that testing 50 individual filaments was sufficient to characterise the entire population.

This agreement also suggests that filament–level properties can be assessed by re-impregnating reclaimed mats with resin films and testing the composites. This requires preserving the original reinforcement architecture and controlling potential re-manufacturing defects, but its significance in an industrial reclamation line (with diverse feedstock) would be far superior to any reasonable SFTT programme.

Figure 13 presents the relation between fibre strength retention and other measured parameters. All plots lack data for moderately strong fibres ($40 - 90\%$), hence the potential of these parameters as fine quality indicators cannot be fully evaluated (this may nevertheless be beyond the needs of commercially viable operations, as discussion in Section 5.7). Measuring the area density of recycled weaves detects both severe fibre degradation (associated with low areal densities) and residual matrix; it is also the only method to determine the loss of carbon fibre during reclamation.

Figure 12 shows that composite performance is extremely dependent on the loading case, and not necessarily effected by filament strength. This is also the case for discontinuous–architecture composites, where fibre strength is not dominant and residual matrix can actually improve performance [10]. There is a strong case to consider different optimisation targets — and, therefore, different quality control strategies — for reclamation processes, based on the application foreseen for the recycled fibres.

5.7. Outlook on commercial CFRP recycling for structural applications

Many fibre reclamation processes have been developed in the last decade and implemented at laboratory or pilot scales. Most methods, including ELG-RCF's pyrolysis, successfully recovered clean fibres with the same properties as the virgin precursors.

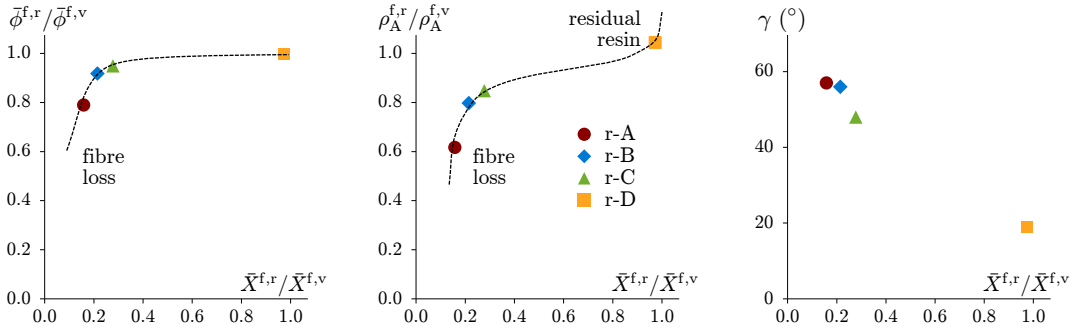

(a) Fibre diameter retention. (b) Area density retention. (c) Maximum manual shear deformation.

Figure 13: Relation between parameters characterising the morphology of recycled weaves and fibre strength retention: experimental observations (data points) and suggested trends (dashed lines).

The results of this work show that commercial–scale recycling is much more challenging. While there is still scope to explore pyrolysis cycles in between processes C and D, there is no guarantee that commercially viable reclamation processes can be tuned finely enough so as to remove all original matrix without inducing any fibre damage, due to the following challenges:

Throughput and processing time. Continuous processes can have running times under 30 min [3], while typical laboratory batch processes report hours for recycling a few grams of composite [4]. To guarantee the same level of matrix removal, the former implies using more aggressive cycles, so risking fibre degradation.

Implementation as a continuous process. In a batch process, the atmosphere and temperature can be precisely tuned. Semi-open conveyor–belt processes [3] require the cycle to be controlled relatively to position rather than time. Guaranteeing ideal and uniform conditions is therefore much more difficult.

Unknown and mixed feedstock. The scrap material used in this work was a specific type of uncured prepreg. Commercial recycling must deal with mixed feedstock and unknown specifications. Aiming for optimal reclamation conditions requires identifying and sorting the feedstock in great detail, which may not be always technically feasible or economically viable.

If one of the two goals of recycling — matrix removal and retention of fibre properties — is to be sacrificed, it is useful to consider the application foreseen for the recycled fibres (as suggested in Figure 12). It must be nevertheless highlighted that aggressive cycles yield a considerable loss of fibre mass (Figure 13b) and, therefore, of profit.

Finally, leaving manufacturing considerations aside, the recycled composites here

analysed exhibited an outstanding retention of mechanical properties relatively to the virgin precursor: approximately 100% for stiffness, up to 80% for tensile strength, and up to 100% of compressive strength. This performance is well above that of aluminium or glass–fibre composites.

6. Conclusions

The mechanical response of several recycled carbon fibres (reclaimed by different pyrolysis cycles at a commercial plant [3]) and woven composites was analysed and compared to that of virgin precursors.

Fibre performance was dramatically affected by the pyrolysis cycle. The most aggressive conditions yielded fibres 21% thinner, with extensive pitting and surface damage, and with 84% tensile strength reduction. The most gentle cycle recovered fibres with virtually no degradation, but left 7.6% of residual resin in the reclaimed fabric.

Two reclaimed weaves were re-impregnated by resin film infusion into recycled woven composites. In the absence of residual resin, the recyclate evidenced similar fibre content and fibre–matrix adhesion to the virgin precursor, showing no need for re-sizing or re-prepreging. Re-manufacturing was more challenging for the weave contaminated by residual resin, but results suggest that imposing pressure during cure is sufficient to achieve a good re-impregnation.

The mechanical performance at composite level was very complex, depending not only on the reclamation cycle but also on the re-manufacturing process and loading case. Tensile strength was dominated by fibre strength, thus favouring the most gentle pyrolysis cycle. Under compression, however, composite strength was insensitive to severe fibre degradation, but considerably affected by the presence of residual matrix. In all cases, composite stiffness (for normalised fibre content) was nearly unaffected.

While CFRP recycling at laboratory scale can reclaim virgin–like fibres, commercially viable implementations will likely operate under non–ideal conditions. This work shows that, if recycled fibres are to be re-introduced in structural components, it is critical to identify potential applications, its loading conditions, and how the intended mechanical response is affected by potential recycling defects.

Acknowledgements

The funding from Portuguese Foundation for Science and Technology (project nr. SFRH/BD/44051/2008) is gratefully acknowledged.

All reclaimed weaves analysed in this work were recycled at Recycled Carbon Fibre Ltd. (now ELG Carbon Fibre Ltd.), UK. The authors would like to acknowledge S. Alsop (Technical Manager) and S. Line (Managing Director) for their contribution.

The authors are also thankful to Cristina Niubó, Júlia Castellà Martín and Yumnah Mohamied for their help with single–fibre and composite testing.

Appendix A. Estimation of single–fibre strength distributions

Due to the brittle nature of carbon–fibres, characterising their strength requires taking into account the associated stochastic variability. An overview of the methods used in this paper for (i) estimating fibre strength Weibull distribution parameters and for (ii) estimating percentile ranks of experimental observations is given below.

Assume that, for each fibre type, the strength of single fibres (X) follows a Weibull distribution, and has a dependency on the gauge length (l) in agreement with the weakest link theory; the effect of stress concentrations at fibre ends is neglected [17]. The single–fibre strength distribution is then characterised by a Cumulative Distribution Function (CDF) and a Probability Density Function (PDF) defined respectively as:

$$\begin{aligned} F_X(\sigma) &= 1 - \exp\left[-\frac{l}{\hat{l}} \cdot \left(\frac{\sigma}{\hat{\sigma}_0}\right)^m \right] \qquad \text{and} \\ f_X(\sigma) &= \frac{\mathrm{d}F_X(\sigma)}{\mathrm{d}\sigma} = \frac{m}{\sigma} \cdot \frac{l}{\hat{l}} \cdot \left(\frac{\sigma}{\hat{\sigma}_0}\right)^m \cdot \exp\left[-\frac{l}{\hat{l}} \cdot \left(\frac{\sigma}{\hat{\sigma}_0}\right)^m \right] \end{aligned} \tag{A.1}$$

where m and $\hat{\sigma}_0$ are respectively the shape and scale parameters, being the latter defined at the reference length $\hat{l}$.

The log–likelihood $\mathcal{L}$ associated with a set $\boldsymbol{\sigma} = \{\sigma_1, \sigma_2, \ldots, \sigma_i, \ldots, \sigma_N\}$ of N strength realisations (each measured at a length l_i, with $i = 1 \ldots N$) is:

$$\begin{aligned} \mathcal{L} &= \ln\left[\prod_{i=1}^{N} f_X(\sigma_i) \right] \\ &= N \cdot \ln(m) + \sum_{i=1}^{N} \ln(l_i) - N \cdot \ln(\hat{l}) + (m-1) \sum_{i=1}^{N} \ln(\sigma_i) - N \cdot m \cdot \ln(\hat{\sigma}_0) - \sum_{i=1}^{N} \frac{l_i \cdot {\sigma_i}^m}{\hat{l} \cdot \hat{\sigma}_0^m} \end{aligned} \tag{A.2}$$

The maximum likelihood estimators of the parameters m and $\hat{\sigma}_0$ define a stationary

point of $\mathcal{L}$, hence verifying:

$$\begin{cases} \dfrac{\partial \mathcal{L}}{\partial \hat{\sigma}_0} = -N \cdot \dfrac{m}{\hat{\sigma}_0} + \dfrac{m}{\hat{\sigma}_0} \cdot \displaystyle\sum_{i=1}^{N} \frac{l_i}{\hat{l}} \cdot \left(\frac{\sigma_i}{\hat{\sigma}_0} \right)^m = 0 \\ \dfrac{\partial \mathcal{L}}{\partial m} = \dfrac{N}{m} + \displaystyle\sum_{i=1}^{N} \ln(\sigma_i) - N \cdot \ln(\hat{\sigma}_0) - \sum_{i=1}^{N} \frac{l_i}{\hat{l}} \cdot \ln\left(\frac{\sigma_i}{\hat{\sigma}_0} \right) \cdot \left(\frac{\sigma_i}{\hat{\sigma}_0} \right)^m = 0 \end{cases} \tag{A.3}$$

Solving the first condition results in the explicit definition of $\hat{\sigma}_0$ as:

$$\sum_{i=1}^{N} \frac{l_i}{\hat{l}} \cdot \left(\frac{\sigma_i}{\hat{\sigma}_0} \right)^m = N \quad \Leftrightarrow \quad \hat{\sigma}_0 = \left(\frac{1}{N \cdot \hat{l}} \sum_{i=1}^{N} l_i \cdot {\sigma_i}^m \right)^{1/m} \tag{A.4}$$

and solving the second condition results in the implicit definition of m as:

$$\frac{N}{m} + \sum_{i=1}^{N} \ln(\sigma_i) - N \cdot \ln(\hat{\sigma}_0) - \sum_{i=1}^{N} \ln(X_i) \cdot \frac{l_i}{\hat{l}} \cdot \left(\frac{\sigma_i}{\hat{\sigma}_0} \right)^m + \ln(\hat{\sigma}_0) \sum_{i=1}^{N} \frac{l_i}{\hat{l}} \cdot \left(\frac{\sigma_i}{\hat{\sigma}_0} \right)^m = 0 \Leftrightarrow$$

$$\overset{\text{Eq. A.4}}{\Leftrightarrow} \quad \frac{N}{m} + \sum_{i=1}^{N} \ln(\sigma_i) - N \cdot \frac{\displaystyle\sum_{i=1}^{N} \ln(\sigma_i) \cdot l_i \cdot {\sigma_i}^m}{\displaystyle\sum_{i=1}^{N} l_i \cdot {\sigma_i}^m} = 0 \tag{A.5}$$

Equations A.4 and A.5 can be used to estimate Weibull parameters m and $\hat{\sigma}_0$ from an experimental data set $\boldsymbol{\sigma}$.

To plot the experimentally obtained CDF of fibre strength, it is necessary to estimate the rank percentile F_X for each strength realisation σ_i. The procedure adopted here was proposed by Gilchrist [30], and is summarised below.

Let $X^{(j,N)}$ (with $j = 1, \ldots, N$) be the j^{th} order statistic of the random sample of size N, with CDF represented as $F_{X^{(j,N)}}(\sigma) = \text{Prob}(X^{(j,N)} \leq \sigma)$. Because the unordered realisations are independent and identically distributed, $F_{X^{(j,N)}}(\sigma)$ can be related to $F_X(\sigma)$ by [30]:

$$F_{X^{(j,N)}}(\sigma) = \sum_{k=j}^{N} \binom{N}{k} \Big[F_X(\sigma) \Big]^k \cdot \Big[1 - F_X(\sigma) \Big]^{N-k} \tag{A.6}$$

The right–hand side of Equation A.6 can be re-written using a binomial distribu-

tion, and thus using the Regularised Incomplete Beta Function I, with parameters $(j, N-j+1)$:

$$F_{X^{(j,N)}}(\sigma) = 1 - \sum_{k=0}^{j-1} \binom{N}{k} \Big[F_X(\sigma)\Big]^k \cdot \Big[1 - F_X(\sigma)\Big]^{N-k} = I\Big(F_X(\sigma);\, j,\, N-j+1\Big) \quad \text{(A.7)}$$

The theoretical median rank for the j^{th} order statistic is obtained when $F_{X^{(j,N)}}(\sigma) = 0.5$. For each experimental realisation $\sigma^{(j)}$ $(j = 1, \ldots, N)$, the median rank $F_X^{[0.5]}(\sigma^{(j)})$ can therefore be estimated as (following Equation A.7):

$$F_X^{[0.5]}(\sigma^{(j)}) = I^{-1}\Big(0.5;\, j,\, N-j+1\Big) \quad \text{(A.8)}$$

Similarly, a confidence interval $(1-\alpha)$ for the CDF of each ordered realisation $\sigma^{(j)}$ can be estimated as:

$$\begin{aligned} &\Big[F_X^{[\alpha/2]}(\sigma^{(j)})\,;\, F_X^{[1-\alpha/2]}(\sigma^{(j)})\Big] \quad = \\ &= \quad \Big[I^{-1}\Big(\alpha/2;\, j,\, N-j+1\Big)\,;\, I^{-1}\Big(1-\alpha/2;\, j,\, N-j+1\Big)\Big]\,, \text{ for } j = 1, \ldots, N \end{aligned} \quad \text{(A.9)}$$

Appendix B. Data reduction for ±45° shear tests considering large deformations

The ASTM standard for ±45° shear tests [20] discards all experimental data for $\gamma_{12} > 5\%$, as the assumptions of a nominal ±45° configuration and negligible exten-

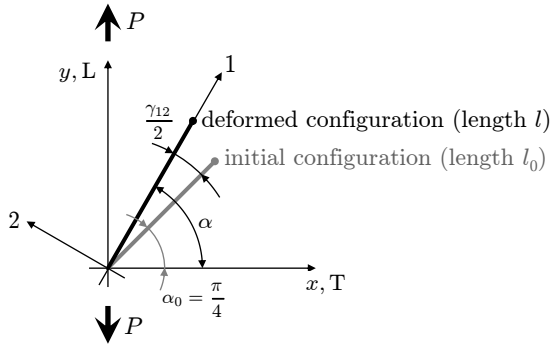

Figure B.14: Kinematics of deformation in an orthogonal 2–D composite during a ±45° shear test.

sional stresses are no longer valid. However, such procedure would hinder the comparison between the performances of recycled and virgin composites. Therefore, a data reduction method accounting for large deformations and fibre extension is proposed.

Figure B.14 represents schematically one quadrant (defined by the two in–plane symmetry axes) of an orthogonal 2–D woven composite during the $\pm 45^{\circ}$ shear test; the initial configuration is represented by the subscript 0, and the tensile load (P) is applied vertically. Let l be the length of a tow crossing the origin and α its angle with the horizontal axis, so that the longitudinal (ε_{L}), transverse (ε_{T}), fibre (ε_1) and shear (γ_{12}) deformations are:

$$\varepsilon_{\mathrm{L}} = \frac{l \cdot \sin(\alpha)}{l_0 \cdot \sin(\alpha_0)} - 1, \quad \varepsilon_{\mathrm{T}} = \frac{l \cdot \cos(\alpha)}{l_0 \cdot \cos(\alpha_0)} - 1, \quad \varepsilon_1 = \frac{l}{l_0} - 1 \quad \text{and} \quad \gamma_{12} = 2 \cdot (\alpha - \alpha_0) \tag{B.1}$$

Combining ε_{L} and ε_{T} with ε_1 yields:

$$\varepsilon_{\mathrm{L}} = \frac{(1+\varepsilon_1) \cdot \sin(\alpha)}{\sin(\alpha_0)} - 1 \qquad \text{and} \qquad \varepsilon_{\mathrm{T}} = \frac{(1+\varepsilon_1) \cdot \cos(\alpha)}{\cos(\alpha_0)} - 1 \tag{B.2}$$

Solving both equalities relatively to ε_1,

$$\varepsilon_1 \; = \; \frac{(1+\varepsilon_{\mathrm{L}}) \cdot \sin(\alpha_0)}{\sin(\alpha)} - 1 \; = \; \frac{(1+\varepsilon_{\mathrm{T}}) \cdot \cos(\alpha_0)}{\cos(\alpha)} - 1 \tag{B.3}$$

and, as $\alpha_0 = \pi/4$ and following the definition of γ_{12} in Equation B.1,

$$\tan(\alpha) = \left(\frac{\varepsilon_{\mathrm{L}} + 1}{\varepsilon_{\mathrm{T}} + 1} \right) \quad \Rightarrow \quad \gamma_{12} = 2 \cdot \operatorname{atan}\left(\frac{\varepsilon_{\mathrm{L}} + 1}{\varepsilon_{\mathrm{T}} + 1} \right) - \frac{\pi}{2} \tag{B.4}$$

In the global coordinate system, only longitudinal stresses (σ_{L}) are applied; being t_0 and w_0 the initial thickness and width of the specimen, and considering the variation of the latter,

$$\sigma_{\mathrm{L}} = \frac{P}{t_0 \cdot w_0 \cdot (1+\varepsilon_{\mathrm{T}})} \tag{B.5}$$

Once γ_{12} (or α) is known, σ_{L} can be rotated to the local material coordinate system, so shear stresses in material coordinates are defined as:

$$\tau_{12} \; = \; \frac{\sigma_{\mathrm{L}}}{2} \cdot \sin(2 \cdot \alpha) \; \overset{\text{Eq. B.1}}{=} \; \frac{\sigma_{\mathrm{L}}}{2} \cdot \sin(\gamma_{12} + \pi/2) \; \overset{\text{Eq. B.5}}{=} \; \frac{P}{2 \cdot t_0 \cdot w_0 \cdot (1+\varepsilon_{\mathrm{T}})} \cdot \cos(\gamma_{12}) \tag{B.6}$$

Appendix C. Estimation of confidence intervals for ratio of means

The effect of recycling on the performance of composites can be assessed by the retention of mechanical properties of the recycled composites relatively to their virgin precursor. The confidence intervals for the retention shown in Figure 9 were calculated from Fieller's theorem [23], as described below.

Consider the experimental measurements of a mechanical property χ (e.g. stiffness or strength). For each material (recycled and virgin composites, here identified with subscripts r and v), the measured average and variance are respectively $\bar{\chi}$ and s^2, and the sample size is N. The (unknown) expected value and variance of the population are represented as μ and σ^2; $\bar{\chi}$ can be assumed as normally distributed.

The retention ratio p and its estimator ($\hat{p}$) are defined as:

$$p = \frac{\mu_\mathrm{r}}{\mu_\mathrm{v}} \qquad \text{and} \qquad \hat{p} = \frac{\bar{\chi}_\mathrm{r}}{\bar{\chi}_\mathrm{v}} \tag{C.1}$$

Let the auxiliary stochastic variable d be defined as:

$$d = \bar{\chi}_\mathrm{r} - p \cdot \bar{\chi}_\mathrm{v} \tag{C.2}$$

Being a linear combination of normal variables, d follows a normal distribution as well, with expected value $\mu_d = 0$ and unknown variance ${\sigma_d}^2$. Standardising,

$$t = \frac{d - \mu_d}{\hat{\sigma}_d} \sim T_{N_d} \quad \text{with} \quad \begin{cases} \mu_d = 0 \\ \hat{\sigma}_d^2 = \dfrac{{s_\mathrm{r}}^2}{N_\mathrm{r}} + p^2 \cdot \dfrac{{s_\mathrm{v}}^2}{N_\mathrm{v}} \end{cases} \tag{C.3}$$

where $T(N_d)$ represents the t–distribution with $N_d = N_\mathrm{r} + N_\mathrm{v} - 2$ degrees of freedom.

Taking the square of Equation C.3 and solving relatively to p,

$$p = \frac{\bar{\chi}_\mathrm{r} \cdot \bar{\chi}_\mathrm{v} \pm t \cdot \sqrt{\dfrac{{s_\mathrm{v}}^2}{N_\mathrm{v}} \cdot \bar{\chi}_\mathrm{r}^2 - t \cdot \dfrac{{s_\mathrm{r}}^2}{N_\mathrm{r}} \cdot \dfrac{{s_\mathrm{v}}^2}{N_\mathrm{v}} + \dfrac{{s_\mathrm{r}}^2}{N_\mathrm{r}} \cdot \bar{\chi}_\mathrm{v}^2}}{\bar{\chi}_\mathrm{v}^2 - t^2 \cdot \dfrac{{s_\mathrm{v}}^2}{N_\mathrm{v}}} \tag{C.4}$$

Taking the positive root and dividing both numerator and denominator by $\bar{\chi}_\mathrm{v}^2$,

$$p = \frac{\bar{\chi}_\mathrm{r}}{g \cdot \bar{\chi}_\mathrm{v}} \cdot \left(1 + t \cdot \sqrt{\frac{{s_\mathrm{v}}^2}{N_\mathrm{v} \cdot \bar{\chi}_\mathrm{v}^2} + g \cdot \frac{{s_\mathrm{r}}^2}{N_\mathrm{r} \cdot \bar{\chi}_\mathrm{r}^2}} \right) \quad \text{, with} \quad g = 1 - t^2 \cdot \frac{{s_\mathrm{v}}^2}{N_\mathrm{v} \cdot \bar{\chi}_\mathrm{v}^2} \tag{C.5}$$

Equation C.5 represents a probability distribution for p. The $(1-\alpha)$ confidence interval for the retention of mechanical performance is thus defined as:

$$p \in \left[\frac{\bar{\chi}_\mathrm{r}}{g \cdot \bar{\chi}_\mathrm{v}} \cdot \left(1 + t_{N_d}(\alpha/2) \cdot c_p\right) \; ; \; \frac{\bar{\chi}_\mathrm{r}}{g \cdot \bar{\chi}_\mathrm{v}} \cdot \left(1 + t_{N_d}(1-\alpha/2) \cdot c_p\right) \right] \quad ,$$

$$\text{with} \quad g = 1 - t^2 \cdot \frac{{s_\mathrm{v}}^2}{N_\mathrm{v} \cdot \bar{\chi}_\mathrm{v}^2} \qquad \text{and} \qquad c_p = \sqrt{\frac{{s_\mathrm{v}}^2}{N_\mathrm{v} \cdot \bar{\chi}_\mathrm{v}^2} + g \cdot \frac{{s_\mathrm{r}}^2}{N_\mathrm{r} \cdot \bar{\chi}_\mathrm{r}^2}} \qquad \text{(C.6)}$$

References

[1] S. Pimenta, S. T. Pinho, Recycling carbon fibre reinforced polymers for structural applications: Technology review and market outlook, Waste Management 31 (2) (2011) 378–392.

[2] S. J. Pickering, Recycling technologies for thermoset composite materials — current status, Composites Part A 37 (8) (2006) 1206–1215.

[3] ELG Carbon Fibre Ltd., `www.recycledcarbonfibre.com` (last accessed March 2012).

[4] L. O. Meyer, K. Schulte, E. Grove-Nielsen, CFRP–recycling following a pyrolysis route: Process optimization and potentials, Journal of Composite Materials 43 (9) (2009) 1121–1132.

[5] J. P. Heil, M. J. Hall, D. R. Litzenberger, R. Clearfield, J. J. Cuomo, P. E. George, W. L. Carberry, A comparison of chemical, morphological and mechanical properties of various recycled carbon fibers, in: SAMPE'09 Conference, SAMPE, Baltimore, MD, USA, 2009.

[6] G. Cornacchia, S. Galvagno, S. Portofino, F. Caretto, Giovanni, Casciaro, D. Matera, A. Donatelli, P. Iovane, M. Martino, R. Civita, S. Coriana, Carbon fiber recovery from waste composites: an integrated approach for a commercially successful recycling operation, in: SAMPE'09 Conference, SAMPE, Baltimore, MD, USA, 2009.

[7] K. H. Wong, S. J. Pickering, T. A. Turner, N. A. Warrior, Compression moulding of a recycled carbon fibre reinforced epoxy composite, in: SAMPE'09 Conference, SAMPE, Baltimore, MD, USA, 2009.

[8] T. A. Turner, S. J. Pickering, N. A. Warrior, Development of high value composite materials using recycled carbon fibre, in: SAMPE'09 Conference, SAMPE, Baltimore, MD, USA, 2009.

[9] M. A. Janney, W. L. Newell, E. Geiger, N. Baitcher, T. Gunder, Manufacturing complex geometry composites with recycled carbon fiber, in: SAMPE'09 Conference, SAMPE, Baltimore, MD, USA, 2009.

[10] S. Pimenta, S. T. Pinho, P. Robinson, K. H. Wong, S. J. Pickering, Mechanical analysis and toughening mechanisms of a multiphase recycled CFRP, Composites Science and Technology 70 (12) (2010) 1713–1725.

[11] J. Meredith, The role of recycled carbon fibre composites in motorsport applications, in: Carbon Fibre Recycling and Reuse Conference, IntertechPira, Hamburg, Germany, 2009.

[12] J. Meredith, S. Cozien-Cazuc, E. Collings, S. Carter, S. Alsop, J. Lever, S. R. Coles, B. M. Wood, K. Kirwan, Recycled carbon fibre for high performance energy absorption, Composites Science and Technology 72 (6) (2012) 688695.

[13] J. P. Heil, D. R. Litzenberger, J. J. Cuomo, A comparison of chemical, morphological, and mechanical properties of carbon fibers recovered from commercial recycling facilities, in: SAMPE 2010 Conference, SAMPE, Seattle, WA, USA, 2010.

[14] Hexcel Corporation, HexPly M56 Product Data, Publication FTA 283 (2008).

[15] Hexcel Corporation, HexTow AS4 Product Data (2010).

[16] British Standards Institution, Implementation of ISO 11566:1996, Carbon fibre — Determination of the tensile properties of single–filament specimens, 1996.

[17] E. G. Stoner, D. D. Edie, S. D. Durham, An end–effect model for the single–filament tensile test, Journal of Materials Science 29 (24) (1994) 6561–6574.

[18] ASTM International, Standard test method for tensile properties of polymer matrix composite materials, ASTM D 3039/D 3039M – 07, in: Anual Book of ASTM Standards, Vol. 08, 2008.

[19] J. G. Haberle, E. W. Godwin, The Imperial College method for testing composite materials in compression , Technical Memo TM 93/03, The Composites Centre, Imperial College London, UK (1993).

[20] ASTM International, Standard test method for in-plane shear response of polymer matrix composite materials by tensile test of a $\pm 45^\circ$ laminate, ASTM D 3518/D 3518M–94, in: Anual Book of ASTM Standards, Vol. 08, 2008.

[21] N. V. De Carvalho, S. T. Pinho, P. Robinson, An experimental study of failure initiation and propagation in 2D woven composites under compression, Composites Science and Technology 71 (10) (2011) 1316–1325.

[22] Hexcel Corporation, HexPly 8552 Product Data, Publication FTA 072c (2008).

[23] W. Dunlap, C. Silver, Confidence–intervals and standard errors for ratios of normal variables, Behaviour Research Methods, Instruments & Computers 18 (5) (1986) 469–471.

[24] M. Karayaka, P. Kurath, Deformation and failure behavior of woven composite laminates, Journal of Engineering Materials and Technology 116 (2) (1994) 222–232.

[25] S. Pimenta, S. T. Pinho, P. Robinson, Hierarchical scaling law for the strength of composite fibre bundles, submitted to the Journal of the Mechanics and Physics of Solids (2012).

[26] C. Schultheisz, A. Waas, Compressive failure of composites, 1: Testing and micromechanical theories, Progress in Aerospace Sciences 32 (1) (1996) 1–42.

[27] N. V. De Carvalho, S. T. Pinho, P. Robinson, Analytical modelling of the compressive and tensile response of 2D woven composites, submitted to Composites Part A (2012).

[28] S. Pimenta, R. Gutkin, S. T. Pinho, P. Robinson, A micromechanical model for kink-band formation: Part II — analytical modelling, Composites Science and Technology 69 (7-8) (2009) 956–964.

[29] R. Gutkin, S. T. Pinho, P. Robinson, P. T. Curtis, A finite fracture mechanics formulation to predict fibre kinking and splitting in CFRP under combined lon-

gitudinal compression and in-plane shear, Mechanics of Materials 43 (11) (2011) 730–739.

[30] W. Gilchrist, Statistical Modelling with Quantile Functions, Chapman and Hall/CRC, USA, 2000.